Metallurgical and Materials Engineering *Scientific paper*
Association of Metallurgical Engineers of Serbia AMES *DOI: 10.30544/244335*

EFFECT OF Mg CONTENTS ON THE MECHANICAL PROPRIETIES AND PRECIPITATION KINETICS IN Al–3.3 WT.% Cu ALLOY

M. Fatmi [1,], A. Ouali [2], A. Djemli [2], T. Chihi [1], M.A. Ghebouli [3], F. Sahnoune [1,2], B. Ghebouli [4], B. Barka [5]*

[1] *Research Unit on Emerging Materials (RUEM), University Ferhat Abbas of Setif 1, 19000, Algeria*
[2] *Department of Physics, Faculty of Sciences, University of Mohamed Boudiaf, M'sila, 28000, Algeria.*
[3] Department of Chemistry, Faculty of Technology, University of Mohamed Boudiaf, M'sila, 28000, Algeria.
[4] *Laboratory of Studies of Surfaces and Interfaces of Solid Materials, University Ferhat Abbas of Setif 1, 19000, Algeria*
[5] *Laboratory of growth and characterization of new semiconductors, Faculty of Technonology, University of Ferhat Abbas, Setif 01, 19000, Algeria*

Received 25.05.2017
Accepted 04.10.2017

Abstract

The effect of additional Mg on the microstructure, mechanical properties, and transformation kinetics during aging in Al–3.3 wt.% Cu alloy was studied. The compositions and microstructure were examined by X-ray diffraction, Differential scanning calorimetry (DSC) and scanning electron microscope (SEM) with energy dispersive X-ray spectroscopy (EDS). The results show that the Mg in the Al–Cu alloy mainly precipitated to the grain boundaries during the process of transformation and formed a ternary Al_2CuMg metallic compound and the rate of discontinuous precipitation reaction decreases with increasing concentration of Mg. The activation energy of crystallization was evaluated by applying the Kissinger equation.

Keywords: Al–Cu–Mg alloys; Discontinuous precipitation; Activation energy; DSC.

Introduction

The aluminum has excellent mechanical properties in the presence of alloying elements, mainly due to the precipitation hardening (e.g., Al–Cu(Mg) alloys). These

* Corresponding author: Messaoud Fatmi, *fatmimessaoud@yahoo.fr*

alloys and materials are widely used in the aeronautics field [1–5]. For a concentration of Cu less than 4%, the Al–Cu and Al–Cu–Mg phase diagrams show the formation of a solid solution α. Increasing the concentration leads to precipitation of copper in the form of Guinier Preston zones (GP1 and GP2) and the first compound Al_2Cu (θ' metastable, then θ stable), and phases (S' metastable, then S stable) in Al–Cu–Mg alloys [6–7].

The precipitation sequence in the Al–Cu–Mg system can be presented as

$$SSSS\ (\alpha_o) \rightarrow GPB \rightarrow S'' \rightarrow S' \rightarrow S \qquad 1$$

where SSSS (α_o) is the supersaturated solid solution obtained after solution treatment and quenching. *S. C. Wang and M. J. Starink*, investigated the effect of heat treatments and deformation on the formation of two variants of S phase precipitation in an Al–4.2Cu–1.5Mg–0.6 Mn–0.5 Si (AA2024) and Al–4.2 Cu–1.5 Mg–0.6 Mn–0.08 Si (AA2324) (wt.%) alloys using transmission electron microscopy (TEM) and a scanning electron microscopy (SEM) analysis [7]. The DSC analysis of the as–solution treated samples shows two distinct exothermic peaks in the range from 250 to 350 °C. An S phase with a composition of Al_2CuMg has been determined as an orthorhombic Cmcm structure with lattice parameters: a_S = 0.400 nm, b_S = 0.923 nm, c_S = 0.714 nm [8–9]. A range of structures has been proposed for GPB, S", S ′, and S as shown in Table 1 [10–14].

Table 1. Previous reported and proposed structures for GPB and S", S' and S phases.

Crystallographic structure	Composition	Experimental data supporting model	Structure name	Reference
Orthorhombic, *a* = 0.405 nm, *b* = 0.906 nm and *c* = 0.725 nm	Al2CuMg	Proposed	GPB	[10, 11]
Tetragonal, *a* = 0.405 nm, *c* = 0.81 nm, P4/nbm	Al2CuMg	FPTEC	GPB	[12]
Monoclinic, *a* = 0.400 nm, *b* = 0.925 nm, *c* = 0.718 nm, *α* = 88.6◦	Al2CuMg	XRD	S"	[13]
Orthorhombic, *a* = 0.405 nm, *b* = 0.405 nm and *c* = 0.81 nm, Imm2	Al2CuMg	TEM	S"	[14]
Orthorhombic, a = 0.400 nm, b =0. 461nm, c =0.718nm, Pmm2	Al2CuMg	HREM	S '	[8]
Orthorhombic, a = 0.400 nm, b =0. 923nm, c =0.714 nm, Cmcm	Al2CuMg	XRD	S	[15]

*XRD: X-ray diffraction, TEM: Transmission Electron Microscopy, FPTEC: First–Principles Total Energy Calculations

Nanodiffraction and HREM technology by *J.C.L. Yan et al.* have been used to determine the crystal structure of the S' phase (Al_2CuMg), and conclude it, at 200 °C for times ranging from 10–10.000 h, there appears to be no difference in crystal structure between S ' and equilibrium S phase [15]. Recent work of *R.K.W. Marceau et al.* show diffusion couple after aging for 5 min at 200 °C in Al–1Cu–0.76Mg and Al–2.18Cu–1.66Mg (wt.%); above a critical Cu content the rapid hardening phenomena diminishes [16].

The aim of this research is to study the effect of Mg content on the microstructure and mechanical properties of Al–Cu alloy. The possible effect mechanism will also be discussed.

Experimental methods

Two commercials purity Al–Cu–Mg alloys ingots have been studied; the compositions are shown in Table 2.

Table 2. Compositions of the alloys (wt.%).

	Element				
	Cu	Mg	Fe	Si	Al
S1	3.3	0.98	0.08	0.01	Bal.
S2	3.3	2.03	0.06	0.01	Bal.

Specimens with the size of 10mm×10mm×12mm were wired-cut from the center of the ingot. The specimens were homogenized at 470ºC for one week and quenched in water. Microstructure, morphologies of fracture surface and compositions of tested alloys were analyzed by Scanning Electron Microscopy (SEM) (JEOL 2000FX) equipped with energy dispersive spectroscopy (EDS). Phase identification of the alloys was further confirmed by analyzing X-ray diffraction patterns generated by PAN alytical X'Pert PRO diffractometer. CuKα radiation and a speed of 1°/min were used. The DSC measurements were performed with a NETZSCH 200 PC DSC. Vickers hardness is one of the most testing techniques and scientists. It is a form of microhardness that uses a diamond indenter and is suitable for a wide range of materials. A Yukon 2500 device was used in the microhardness measurements.

Results and discussion

The as-quenched microstructure

The as-quenched microstructures are shown in Fig. 1. It is a typical structure that consists of the fine precipitates with a grain boundary. Fig. 2 represents a typical EDS spectrum of the presents alloys in the as-quenched condition. The quantitative analysis of six different EDS spectra indicated that the average chemical compositions were: Al–3.3±0.3 wt.%–Cu–0.96±0.2 wt.% Mg and Al–3.28±0.1 wt.% Cu–1.98±0.4 wt.% Mg respectively.

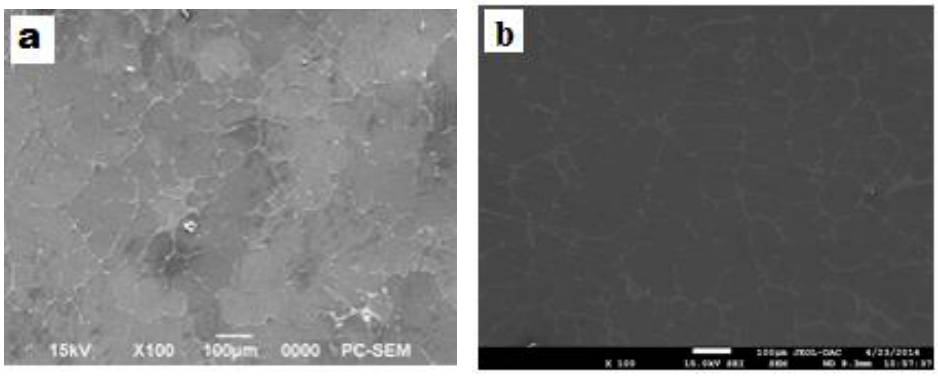

Fig. 1. Microstructures of as-quenched Al–3.3wt.%Cu–1wt.%Mg (a) and Al–3.3wt.%Cu–2wt.%Mg (b) alloys.

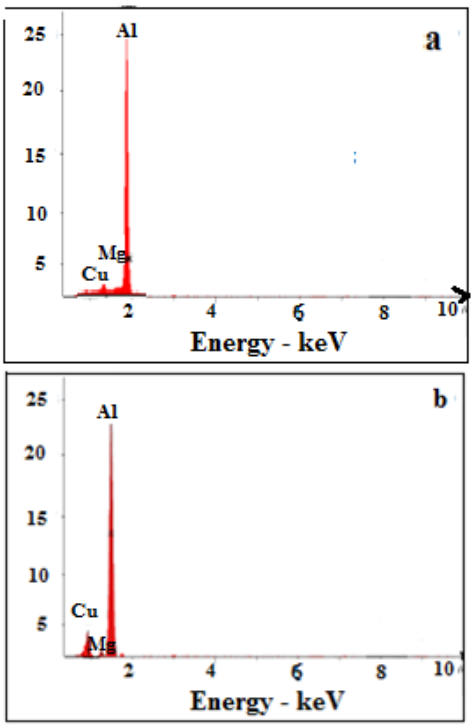

Fig. 2. A typical EDS profile of Al–3.3wt.%Cu–1wt.%Mg (a) and Al–3.3wt.%Cu–2wt.%Mg (b) alloys in the as-quenched conditions.

For studying the heat treatment effect on the discontinuous precipitation in Al–3.3wt.% Cu–1 wt.% Mg and Al–3.3 wt.% Cu–2 wt.% Mg alloys, the samples are homogenized at 470 °C for one week and quenched in water. In this part of the investigation, we present the results of differential scanning calorimetry (DSC) in

nonisothermal conditions, previously homogenized and quenched (Fig. 3 and Fig. 4); and age at different heating rates (2, 5, and 10 °C/min).

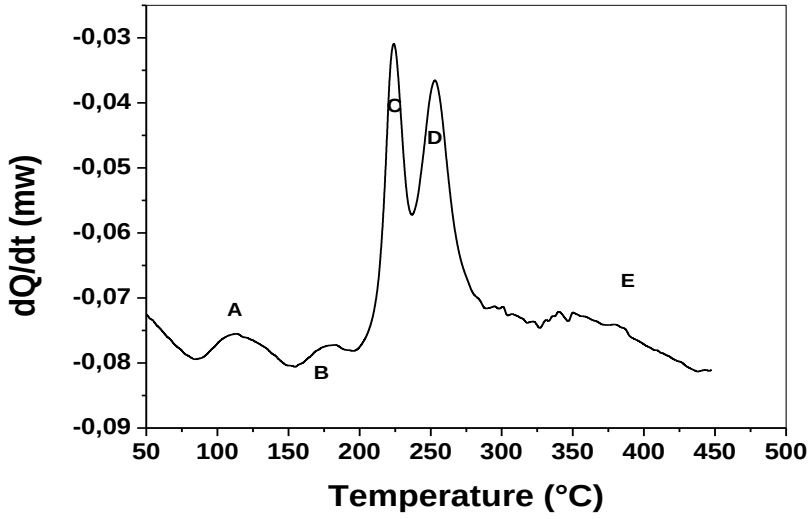

Fig. 3. DSC curve of Al–3.3wt.%Cu–1wt.%Mg alloy, homogenized one week at 470 °C, quenched in water and heated in the range 25 – 450 °C (heating rate 2 °C·min^{-1}).

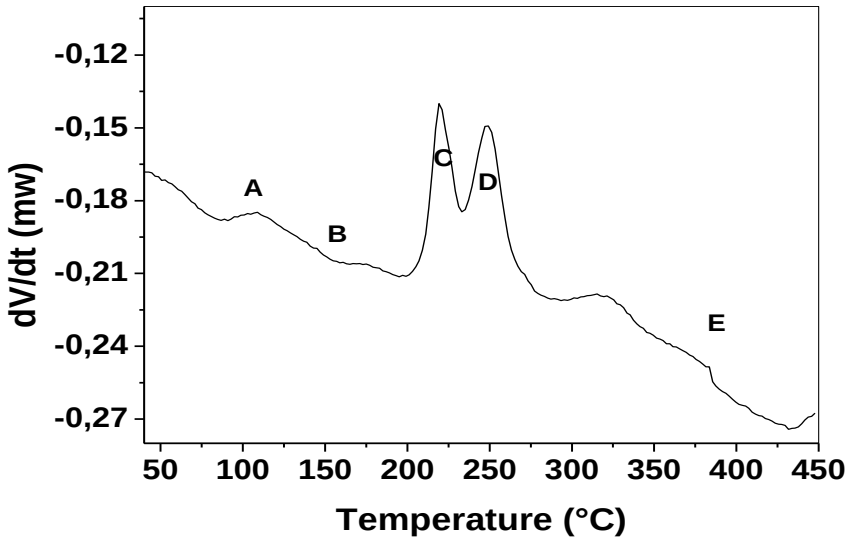

Fig. 4. DSC curve of Al–3.3wt.%Cu–2wt.%Mg alloy, homogenized one week at 470 °C, quenched in water and heated in the range 25 – 450 °C (heating rate 2 °C·min^{-1}).

Five main effects may be identified in these thermograms [17–19] an exothermic peak; A, between 60 and 130 °C that occurred due to the formation of co–clusters [20, 21]; an endothermic effect, B, between 130 and 170 °C, may be attributed to Cu–Mg co–cluster dissolution (with possibly some GPB2 dissolution); two exothermic peaks effect, C, and D between about 200 and 300 °C, are attributed to the formation of S' and S phases precipitates respectively; a broad endothermic effect, E, at 300 to 450 °C is identified as progressive dissolution of the S' and S precipitates [22, 23].

To determine the activation energy E_a of S‘ and S phases of our alloys we use the Kissinger method, this method relies on the assumption that, during the temperature increase, the reaction passes through a maximum before decreasing, using the following relation [24]:

$$\ln\left(\frac{V}{T_m^2}\right) = -\frac{E_a}{T_m \cdot R} + C \qquad 2$$

where C is constant, at the maximum rate of transformation which corresponds to the maximum at the DSC peak $T = T_m$ ($d^2y/dt^2=0$) and R, the perfect gas constant (8.314 J/mol·K).

The maximum temperatures of reactions were determined from the slopes of the DSC curves. The activation energy for the formation of the S‘ and S phases (Al2CuMg) under nonisothermal conditions was calculated from the slope of $\ln\left(\frac{V}{T_m^2}\right)$ – function of 1/Tm.

The value of E_a may be calculated from the slope of each curve it is shown in this following Table 3; these values are in good accordance with the literature [25].

Table 3. The activation energies of S' and S phases of Al–3.3wt.%Cu1wt.%Mg and Al–3.3wt.%Cu2wt.%Mg alloys.

	Phase	E_a(kJ/mol) study
Al–3.3%Cu1%Mg	S'	150.71±2.44
	S	158.44±1.62
Al–3.3%Cu2%Mg	S'	151.82±1.99
	S	157.82±2.05

The results of the heating rate and Mg concentration effect on precipitation are presented in the relative volume fraction versus temperatures (Fig. 5), this figure shows sigmoidal curves at different temperatures for the discontinuous precipitation (DP). It is clear that as the concentration of Mg increases, the rate of DP reaction decreases (shift curves on basis temperatures).

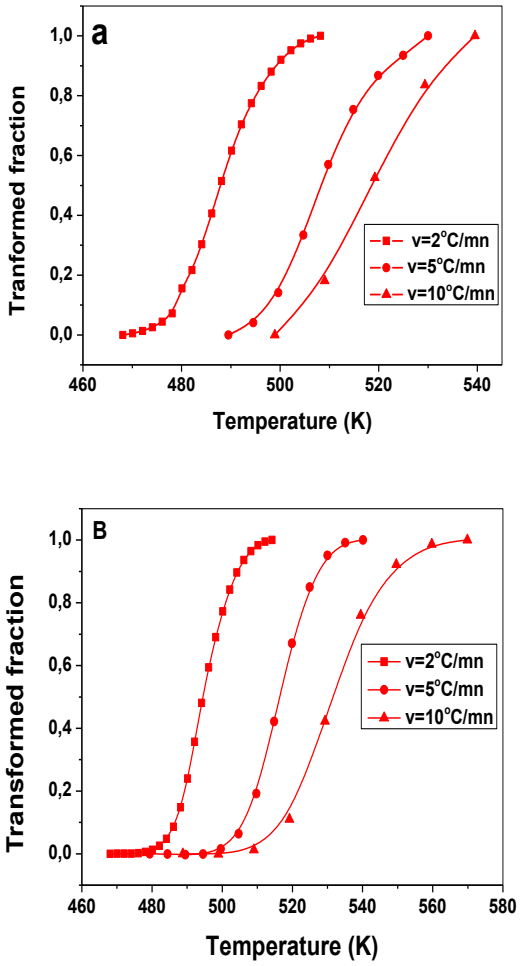

Fig. 5. Transformed fraction as a function of the temperature at various heating rate of Al–3.3wt.%Cu–1wt.%Mg (a) and Al–3.3wt.%Cu–2wt.%Mg (b) alloys of S′ phase.

To determinate the Avrami exponent we used the formula, $n = \frac{2.5R}{\Delta T\ E_a} T_m^2$ [26]:

where are: ΔT – The width at half maximum, E_a– activation energy and R – ideal gas constant.

The Table 4. shows the values of Avrami exponent (n). Avrami analysis was utilized to study the overall bulk crystallization kinetics after a specific thermal history. The Avrami exponent evaluated empirically, generally between 1 and 4. In the present study, the mean value of Avrami coefficient (n) for S' and S phases is 1.41 and 1.42 respectively; which may correspond to phase transformation mechanism driven by the diffusion. It has been found, that like any other diffusion controlled nucleation and growth

process, the reaction front velocity in DP usually records an 'inverse-C' variation with temperature [27].

Table 4. Avrami exponent of S' and S phases of Al–3.3wt.%Cu1wt%Mg and Al–3.3wt.%Cu2wt.%Mg alloys.

Alloy	Al–3.3% Cu–1% Mg		Al–3.3%Cu–2%Mg	
Phase	S'	S	S'	S
n	1.50	1.31	1.46	1.37

It is suggested that atomic mobility is essential for the time-dependent nucleation. It is noticed that the peak moves towards basis temperatures as much as the concentration of Mg increases.

After DSC treatment

The nonisothermal treatment effect on the transformation of precipitation in Al–3.3wt.%Cu1wt.%Mg and Al–3.3wt.%Cu2wt.%Mg was examined before and after DSC treatments. The initial samples are homogenized at 470°C for one week and quenched in water. The X-ray diffraction spectrum of this quenched alloy which corresponds to supersaturated solid solution α_0 is shown in Fig. 6 (a). The second nonisothermal treatment applied on quenched alloy is performed by DSC analysis, from room temperature to 470 °C with heating rate 2 °C/min. The DSC curves show an exothermal peak that corresponds to energy dissipation during the discontinuous precipitation. The formation of this new S phase after last treatment is detected by the X-ray diffraction, where the S phase (Al_2CuMg) peaks are present in the spectrum, Fig. 6 (b, c).

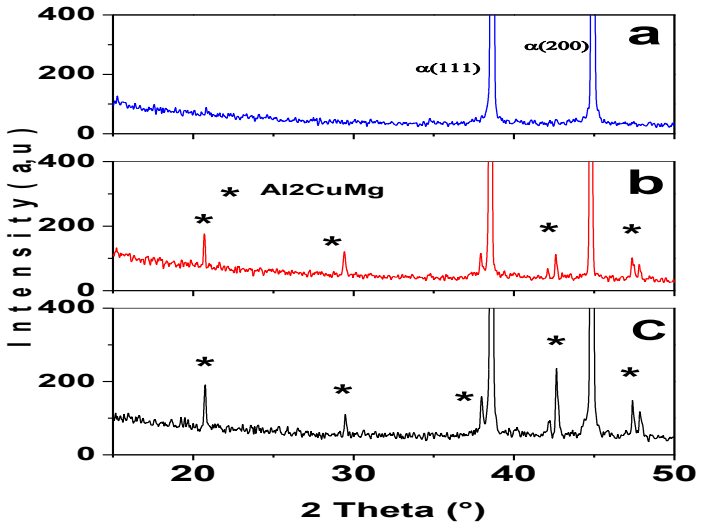

Fig. 6. X-ray diffraction spectrum of Al–3.3wt.%Cu–1wt.%Mg alloy, homogenized at 470 °C for one week and quenched in water (a), after DSC treatment (25–450 °C, v=2 °C.min^{-1}) of Al–3.3wt.%Cu1wt.%Mg (b), and Al–3.3wt.%Cu2wt.%Mg (c) alloys.

However, differential scanning calorimetry (DSC) and XRD analysis, justifies the precipitation of new phases corresponding to the intermetallic phases S′ and S (Al_2CuMg). The grain size has not changed in the same grains observed in the quenched state (bellow DSC treatment). The SEM and EDS analysis revealed these precipitates of different types marked with B and C in Fig. 7. The chemical compositions of the phases are presented in the correspondent EDS curves. The phase marked by B and C is found to have the following composition: 14% Cu, 10% Mg and balance Al and 40% Cu, 3% Mg and balance Al of Al–3.3wt.%Cu1wt.%Mg and Al–3.3wt.%Cu2wt.%Mg respectively, which is consistent with the S phase.

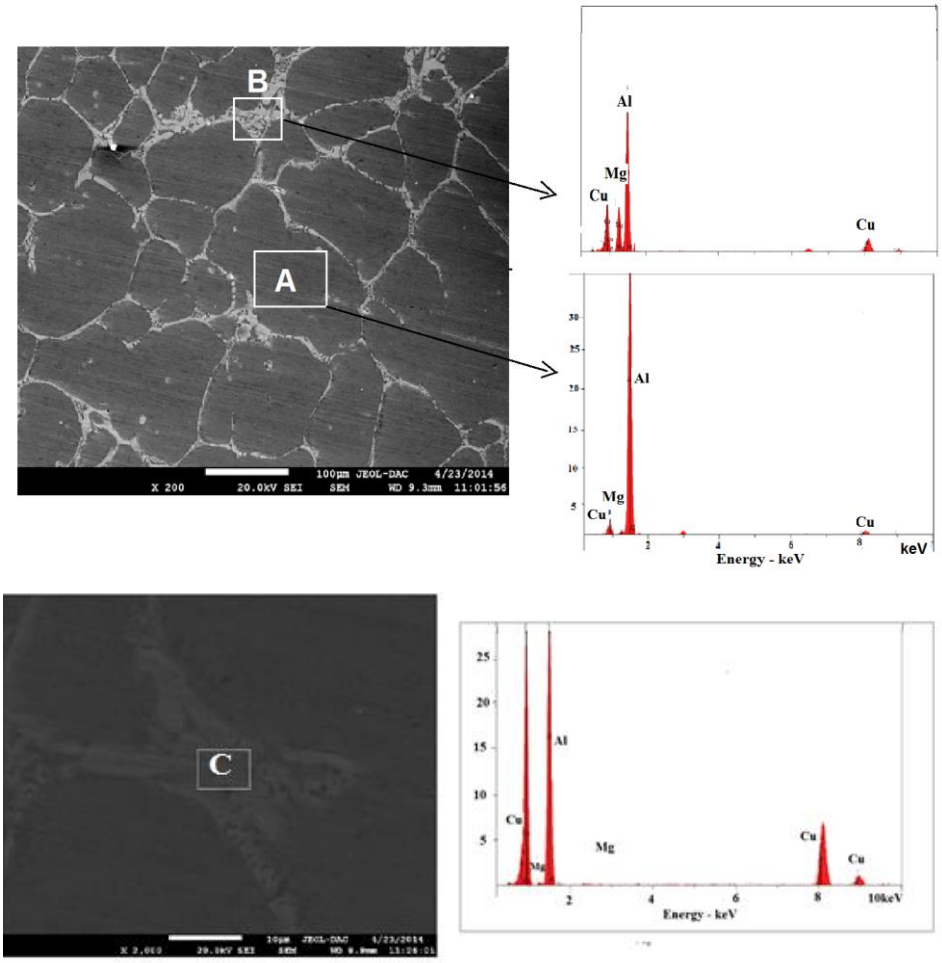

Fig. 7. Microstructures and typical EDS profiles of Al–3.3wt.%Cu–1wt.%Mg alloy marked by A and B and Al–3.3wt.%Cu–2wt.%Mg alloy marked by C (After DSC treatment).

Based on the Al–Cu–Mg phase diagram [28], the solid solubility of Mg is relatively low at room temperature in aluminum alloys. Therefore, the concentration of Mg at the interface of the solid/liquid phases was certain increased correspondingly during the solidification proceeds.

The Vickers hardness value of Al– 3.3wt.%Cu–1 wt.%Mg and Al–3.3wt.%Cu–2 wt.%Mg alloys are presented in Table 5. All samples are aging for various time at 150 ºC . Vickers hardness measurements were carried out in order to investigate the effect of mechanical properties with the small addition of magnesium. The Vickers hardness value of sample of Al–3.3wt.% Cu–2wt.% Mg alloy is slightly lower than that of Al– 3.3wt.% Cu–1 wt.% Mg alloy. We concluded that the hardening observed is due to the formation of the phase S' which is converted into the hardening phase S in order to obtain the maximum hardening in these alloys. values of the microhardness with the prolongation of aging at 150 °C, is directly attributed to the decrease in the amount of precipitated phases and in particular, the metastable phase S 'and the precipitation of equilibrium phases S. The study of Eskin [29] explained the hardening and precipitation in the Al-Cu-Mg-Si alloying system. The composition and hardening phase in Al-Cu-Mg-Si alloys containing 2.5% - 4.5% Cu, are considered with respect to the chemical composition of the supersaturated solid solution.

Table 5. The value of Vickers hardness as a function of aging time at 150 °C of Al–3.3wt.%Cu–1wt.%Mg and Al–3.3wt.%Cu–2wt%Mg alloys.

	Hv (Kg/mm^2)	
Aging time /min.	Al–3.3%Cu1%Mg	Al–3.3%Cu2%Mg
0	109.72±2.35	109.62±2.33
300	115.00±2.22	113.5±2.14
600	115.20±2.12	114.30±2.15
1200	116.05±3.01	114.70±2.35
1800	118.31±3.11	115.20±1.98
2400	123.11±2.63	114.95±1.99
3000	125.21±2.41	117.32±2.09

Conclusion

In this work, the small contents of magnesium and the heating rate of the nonisothermal transformation in the alloy Al–3.3wt.%Cu was studied. Several experimental methods suited to this kind of scientific research, to follow the various structural, and to try to understand the kinetics of various phenomena that occur was used Magnesium in the Al–Cu alloy mainly precipitated to the grain boundaries during the process of transformation and formed ternary Al_2CuMg phase. The DSC curves show the formation two phases S 'and S, with a mean activation energy 154.57 and 154.82 kJ/mol for Al–3.3wt.%Cu–1wt.%Mg and Al–3.3wt.%Cu–2wt.%Mg, respectively. The value of Avrami coefficient (n) for S' and S phases is 1.4; which may correspond to a phase transformation mechanism driven by the diffusion. The rate of discontinuous precipitation reaction decreases with the concentration of Mg increases.

References

[1] G. B. Brook: Precipitation in Metals, Special Report No. 3, Fulmer Research Institute, UK, 1963.
[2] G. B. Brook, B. A. Hatt: The Mechanisms of Phase Transfer in Crystal Solids, Manchester, Institute of Metals, London, 33, 1969, 82.
[3] S. Schumann, H. Friedrich, Magnesium Alloys 2003, Materials Science Forum, 2003, 51: 419– 422.
[4] L. Schlapbach, A. Zuttel: Nature, 414, 6861 (2001) 353–358.
[5] S. P. Ringer, G. R. Quan, T. Sakurai: J Mater Sci Eng A, 250 (1998) 120–126.
[6] A. Somoza, A. Dupasquier, I. J. Polmear, P. Folegati, R. Ferragut: Phys Rev B, 61 (2000) 14454-14463.
[7] S. C. Wang, M. J. Starink: Acta Materialia, 2007, 55:933–941
[8] H. Perlitz, A. Westgren: Arkiv Kemi Mineral Geol B, 16 (1943) 1.
[9] S. C. Wang, M. J. Starink: J Mater Sci Eng A, 386 (2004) 156–163.
[10] F. Cuisiat, P. Duval, R. Graf: Scr Metall, 18 (1984) 1051–1056.
[11] L. F. Mondolfo: Aluminum Alloys, 518 (1976).
[12] C. Wolverton: Acta Mater, 49 (2001) 3129–3142.
[13] T. V. Shchegoleva, N. N. Buinov: Soviet physics**,** crystallography**,** 12 (1967) 552–555.
[14] H. Liang, T. Kraft, Y. A. Chang: J Mater Sci Eng A, 292 (2000) 96–103.
[15] J. Yan, L. Chunzhi, Y. Minggao, J. C. L. Yan, Y. Minggao: J Mater Sci Lett, 9 (1990) 421–424.
[16] R. K. W. Marceau, C. Qiu, S. P. Ringer, C. R. Hutchinson: J Mater Sci Eng A, 546 (2012) 153–161.
[17] M. J. Starink: Int Mater Rev, 49 (2004) 191-226.
[18] F. Lefebvre, S. C. Wang, M. J. Starink, I. Sinclair: Mater Sci Forum, 1555 (2002) 396–402.
[19] S. C. Wang, F. Lefebvre, J. L. Yan, I. Sinclair, M. J. Starink: J Mater Sci Eng A, 431 (2006) 123–136.
[20] H. Lu, P. Kadolkar, K. Nakazawa, T: Ando, C. A. Blue: Metall Mater Trans A, 38 (2007) 2379–2388.
[21] S. C. Wang, M. J. Starink, N. Gao: Scr Mater, 54 (2006) 287–291.
[22] N. Chobaut, D. Carron, J. M. Drezet: J Alloys Compd, 654 (2016) 56–62.
[23] N. Khan, M. J. Starink: Mater Sci Forum, 277 (2006) 519–521.
[24] H. E. Kissinger: Analytical Chemistry, 29 (1957) 1702-1706.
[25] J. L. Yan: Strength Modelling of Al-Cu-Mg Type Alloys, PhD Thesis. University of Southampton; 2006. https://eprints.soton.ac.uk/68691/1/Jialin_Yan_PhD_thesis.pdf
[26] J. A. Augis, J. E. Bennett: J Therm Anal Calorim, 13 (1978) 283–292.
[27] I. Manna, S. K. Pabi, W. Gust: Int Mater Rev, 46 (2001) 53–91.
[28] S. C. Wang, M. J. Starink: Int Mater Rev, 50 (2005) 193–215.
[29] D. G. Eskin: Mater Sci Forum, 396, (2002) 917-922.